A Numerical Investigation of Arctic Ocean Dynamics

J. A. GALT[1]

Dept. of Oceanography, Naval Postgraduate School, Monterey, Calif. 93940

(Manuscript received 19 February 1973, in revised form 25 June 1973)

ABSTRACT

A barotropic numerical model of the Arctic Ocean is formulated to include irregular basin shape, variable bathymetry, lateral friction, bottom drag, and nonlinear advection terms. Source-sink distributions around the perimeter of the basin are used to represent exchange between the Arctic and other portions of the world ocean and the actual bathymetry is parameterized to simulate the effects of weak stratification. The model ocean is spun up using averaged annual wind stress distributions for the Arctic and numerically simulated under-ice stress distributions.

A number of computer runs were made using what were thought to be appropriate parameter ranges for the Arctic. The controlling dynamics in the development of the circulation was discussed for a number of cases and some comparisons made between the model results and observed circulation patterns.

The results of the investigation indicate that topographic Rossby waves play a dominate role in the development and maintenance of general circulation of the Arctic. The intensification of the Beaufort Gyre along the north coast of Alaska is seen to be dynamically similar to the western boundary currents found in mid-latitude oceans, the major difference being that bathymetric variations take over the significance that variations in the Coriolis parameter assume in mid-latitude cases.

1. Introduction

The object of this study was to begin a numerical investigation of the large-scale circulation of the Arctic Ocean.

In the past numerical models of the Arctic Ocean have concentrated their attention on the sea ice that overlies most of the Ocean (Campbell, 1965) and tried to answer questions concerning the drift and climatological permanence of the pack ice (Maykut and Untersteiner, 1971). With the exception of Campbell's use of a simplified ocean model under an ice-layer model, no efforts directed toward a numerical study of the actual flow of the Arctic Ocean's waters have been reported, although there are studies along these lines being conducted at the NOAA Geophysical Fluid Dynamics Laboratory at Princeton, N. J. (Semtner, 1972, personal communication).

At the onset of the research it must be admitted that very little is actually known about Arctic Ocean dynamics and that difficulties can be anticipated in deciding on appropriate boundary conditions and input parameters for the model. In many cases field data from the Arctic are lacking or inadequate to give the required stress fields of inflow-outflow conditions with sufficient accuracy. This then demands that best estimates of boundary conditions serve as a tentative guide and that wide ranges of parametric inputs actually be investigated. The resulting numerical exploration can then yield considerable insight into the relative significance of various oceanographic parameters.

In addition to the uncertainties related to the lack of actual input data, the development of a new numerical model has potential difficulties inherent in the finite-difference mathematics that must be used. Both these problems can best be addressed by the careful development of the model from simple to more complex cases in a stepwise progression with each step being checked against all available data (from the field or by analytic considerations).

The first step in the model to be used for the Arctic assumes homogeneous water and variable depth which is in some way similar to a model used by Holland (1967). The grid system used is based on a triangular plan similar to some systems used by Williamson (1968) and Sadourny *et al.* (1967). Both lateral and bottom friction are included in the model. The flow is driven by stress applied at the surface (simulating the wind or ice stress) and by source-sink distributions around the edge (that simulates major channels between the Arctic and other oceans). The details of the development for the model are given in Section 3.

In Section 4 a description of some of the computer runs exploring parametric variations will be presented and in Section 5 some of the dynamics elucidated by the model will be discussed. Prior to the actual formulation of the model equations some consideration must be given to the roll that sea plays in the circulation of the Arctic Ocean.

It is perhaps appropriate to point out that the next

[1] Present affiliation: NOAA-Pacific Ocean Laboratory, University of Washington, Seattle.

section is largely a development of how an ice cover might modify the length and time scales of thermohaline and wind stress forcing and is not strictly necessary to the continuity of the present work. Therefore, if the reader is only interested in the numerical methods employed and the results of the present mode, the next section could be skipped. On the other hand, it is felt by the author that pack ice does significantly affect the circulation in the Arctic and that the dynamics of this process is essentially unique to the Arctic ocean. Section 2, then, is included in an attempt to point out some of the actual dynamics that are important in the Arctic, to help clarify some of the fundamental limitations of the present model, and to suggest what might be profitable avenues for future model development and exploration.

2. Significance of an ice cover

There can be little doubt that much of the large-scale circulation of the Arctic Ocean is wind driven, either directly or indirectly through an ice cover that acts as some sort of coupling element (Campbell, 1965). The details of how the ice cover couples the atmosphere to the ocean and to what extent it filters the time and space variations are unknown. It should be possible, however, to get a qualitative feeling for the types of interactions possible by a simplified consideration of the physical processes acting.

We may start by considering the vorticity balance for an ice-covered ocean. The curl of the wind field leads to a torque from the wind stress which will be applied to the top of the ice. The ice will then spin-up in some sense and its motion relative to the water underneath will produce the stress that drives the ocean. The ice then might be expected to introduce some delay in time and a smoothing in space for the transmission of torque from the atmosphere to the ocean. How much delay and how much smoothing will depend on the nature of the wind curl.

To see how the ice filter characteristics will depend on the wind field we must think about the structure of the pack ice. It is made up of a number of individual flows. The actual size distribution of the ice flows is fairly complicated but for the problem at hand we need only state that at all times of the year cracks appear every few kilometers or less.

First consider a case with positive curl in the wind stress. Under these conditions the movement of the ice will generally be divergent. (Under some conceivable models for the atmospheric boundary layer this may not be true, but for this qualitative argument we can proceed with the above as an assumption.) With a divergence in the ice field the flows separate, leaving leads or polynyas. The cracks between flows offer no resistance to tension on the pack ice and the divergence takes place rapidly, thus transferring time scales longer than a few hours almost directly from the wind to the water. In addition, a polynya, during the winter, is a region of very high surface cooling; this results in vertical convection which is particularly effective at carrying momentum across the mixed layer. This again tends to directly couple the air and water with almost no change in length scale because of the ice.

Next we consider the case where the wind has a negative curl. Under these conditions the movement of the pack ice will tend to be convergent. The ice flows will jam together and rotate as a single piece. Basically the ice flows show considerable resistance to compression and nearly solid-body rotation of the pack ice over hundreds of kilometers has been observed under anticyclonic wind fields (Bushuyev *et. al.*, 1967). Thus, negative curl in the wind field is transferred to the ocean with the pack ice acting as a fly wheel. Both time and space scales are extended and the stress applied to the water represents a considerable smoothing of the actual wind stress pattern.

Thus far we can see that the ice acts in some ways like a rectifier. Positive stress curl from the wind is transferred more or less directly to the water while for negative stress curl the higher frequencies and shorter length scales are smoothed out. Before discussing the implications of this suggestion one additional case should be considered.

If the convergence or the resulting shear stresses in the pack ice become great enough, mechanical failure takes place and pressure ridges form with large shears often developing across leads. This results in a stress field on the ocean very different from the one suggested by the rectifier analog. In this case large-scale stress fields from the wind are delivered to the ocean during the mechanical failure, and length and time scales are likely to be very much shorter than those found in the wind stress pattern.

Thus, it is possible for the hypothetical ice filter to have a very complicated nature, in some cases increasing the effective length scales in the wind field and in other cases shortening them. The response that we expect from the ocean will be quite different for these two options. The relevant length scale for the problem turns out to be what might be thought of as the internal Rossby deformation length

$$L^2=\frac{\Delta\rho}{\rho}\frac{gh}{f^2},$$

where g is the acceleration of gravity, f the Coriolis parameter, h the geometric mean of the depths above and below the pycnocline, ρ the density, and $\Delta\rho$ the density difference across the pycnocline. [Some authors prefer to relate L to the internal Froude number (e.g., Holton, 1965).] Physically this length can be thought of as how far an internal wave will travel in an inertial period. For the Arctic the stratification is weak and f is relatively large, giving L on the order of tens of kilometers. If the stress field applied to the ocean is

large compared to L, the transient response will be primarily barotropic and if it is small compared to L, a baroclinic response can be anticipated (Veronis and Stommel, 1956).

Over much of the Arctic Ocean and particularly the Canadian side of the Lomonosov Ridge the wind field is anticyclonic and here then we find a convergent ice pack.

There is some evidence that the very short length scales associated with fractures are effective at forcing a transient baroclinic response in the Canadian Arctic (Galt, 1967; Coachman and Newton[2]). Significant shear stresses with a length scale of tens of kilometers or less are relatively rare in the oceans. They occur under hurricanes and in coastal upwelling regions, and in both cases result in significant baroclinic transients. For the Arctic case the actual dynamics of how these transients occur and the ultimate disposition of their energy and its interaction with the mean circulation represents an interesting and as of yet an unanswered question. The flow is fundamentally baroclinic and the present study will not be able to shed any light on its characteristics.

For most of the Arctic for a majority of the time it appears that these baroclinic transients are not present and the stress delivered to the ocean is smoothed and most of the transients occur initially as barotropic waves (Somov, 1954–55; Coachman and Newton[2]). For these kinds of conditions ice models have been fairly successful using either highly viscous compressible flow (Campbell, 1965), or incompressible invisid flow (Rothrock, 1972; Witting, 1972). In all these models the ice effectively interacts over relatively large length scales and realistic looking flow patterns are generated. In the same vein one might expect that a barotropic model of large-scale ocean spin-up and circulation could add some insight into Arctic dynamics. This is the motivation for the presentation of this research.

3. Development of the numerical model

When one considers the actual complexity of the circulation in the Arctic Ocean and the wide variety of numerical modeling techniques available for its study it is by no means obvious which path will lead to maximum returns. Each of the presently used numerical models has its advantages and limitations. In an attempt to address this question in a rational way it was decided to start with the simplest numerical model that could simulate what are thought to be the dominant forcing and geomorphology in the Arctic.

Studies by Coachman and Barnes (1961, 1963) and Aagaard (1966) all indicate that there may be dynamically significant exchange between the Arctic Basin and the adjacent portions of the world ocean. For this reason the numerical model incorporates sources and sinks of water around its perimeter to simulate the major channels between the Arctic and the adjacent parts of the ocean.

Looking at Fig. 1, it is seen that a large fraction of the Arctic is covered by the relative shallow Siberian Shelf, while the deeper portion of the Arctic Ocean is divided into two basins (both over 4000 m deep) by the Lomonosov Ridge. In an attempt to retain some of the dynamical effects caused by these large bathymetric variations the model includes variable depth.

It is likely that the density variations in the Arctic Ocean affect the flow. For example, a full treatment of the movement in the Atlantic layer (Coachman and Barnes, 1963) will certainly require a baroclinic model. On the other hand, there are some actual current measurements from the Arctic (Nikitin and Dem'yanov, 1965; Galt, 1967; Coachman, 1969) that indicate a substantial barotropic, or depth-independent, component to the currents. This coupled with a consideration of the great increase in complexity required for variable density models suggests that for the initial numerical exploration a homogeneous or barotropic formulation be used.

The circulation in the Arctic is not well enough known to come up with an accurate appraisal of the significance of frictional forces. It seems likely that near source-sink points lateral friction could affect the flow. Over the large area covered by the Siberian Shelf it is quite possible that bottom friction might also be significant. Accordingly both lateral and bottom friction were included in the model and it was anticipated that some range of frictional parameters would be investigated to test for significance.

To develop a model with the characteristics described above, the following integrated form of the equations of motion are used:

$$\frac{Du}{Dt}-fv=-\frac{1}{\rho}\frac{\partial P}{\partial x}+K\nabla^2 u-\frac{Ru}{h}+\frac{\tau^x}{\rho h}, \tag{1}$$

$$\frac{Dv}{Dt}+fu=-\frac{1}{\rho}\frac{\partial P}{\partial y}+K\nabla^2 v-\frac{Rv}{h}+\frac{\tau^y}{\rho h}, \tag{2}$$

where the dependent variables u and v are the horizontal components of velocity which are independent of depth. The density ρ is a constant; τ^x and τ^y, the components of the wind stress, h the depth, and f the Coriolis parameter are functions of position; K and R are constants that specify the effectiveness of the horizontal and vertical frictional forces respectively.

In addition to these equations of motion we have the continuity equation:

$$\frac{\partial}{\partial x}(hu)+\frac{\partial}{\partial y}(hv)=0. \tag{3}$$

[2] Personal communication.

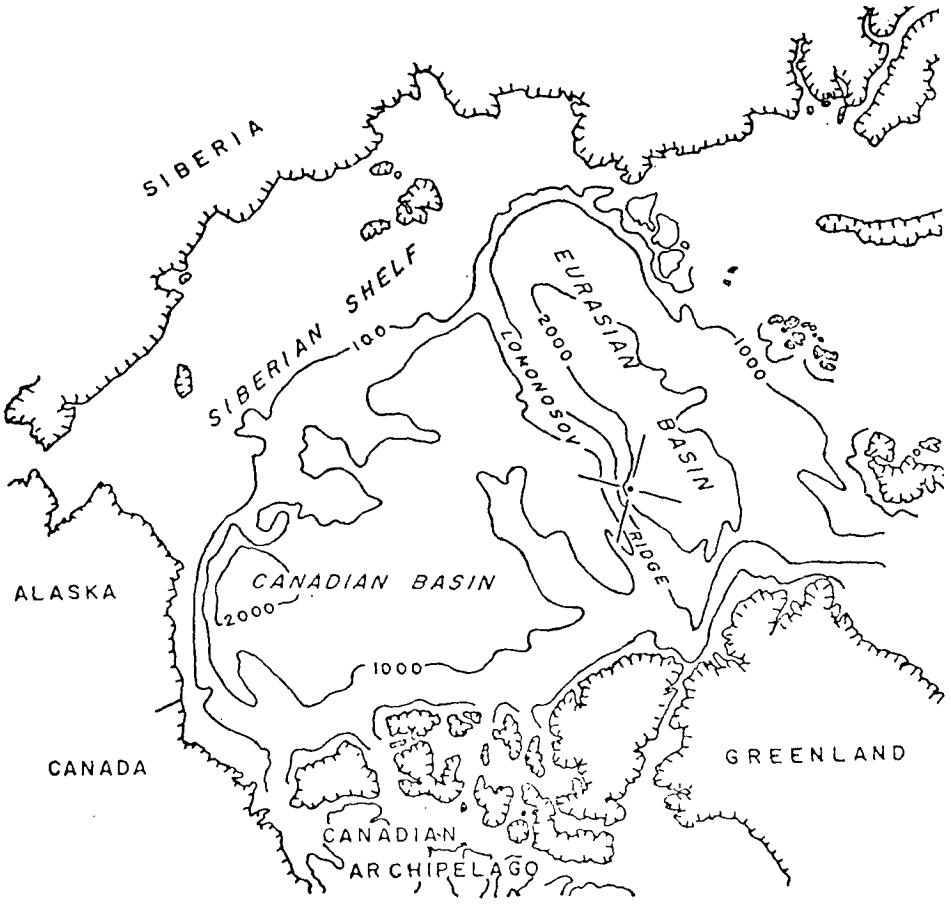

FIG. 1. Chart of Arctic Basin with 100, 1000 and 2000 fathom depth contours. Cross indicates location of North Pole.

A transport streamfunction is introduced such that

$$\left.\begin{aligned} -hu &= \frac{\partial \psi}{\partial y} \\ hv &= \frac{\partial \psi}{\partial x} \end{aligned}\right\}. \tag{4}$$

Eqs. (1)–(4) can be nondimensionalized by introducing the variables

$$\left.\begin{aligned} t &= t'\left(\frac{1}{F}\right), & f &= f'F \\ x &= x'\Delta, & y &= y'\Delta \\ h &= h'D, & \tau &= \tau'\left(\frac{\rho F \psi_0}{\Delta}\right) \\ \psi &= \psi'\psi_0, \end{aligned}\right\}, \tag{5}$$

where the primed quantities are all nondimensional, F is the maximum value of the Coriolis parameter, Δ the finite-difference grid spacing, D the average depth of the model, and ψ_0 is equal to the maximum range of streamfunction on the boundary of the model, or the maximum value expected for the wind-driven portion of the flow, whichever is the most convenient. Using the new variables defined above, the following vorticity equation can be obtained:

$$\frac{\partial \xi'}{\partial t} - (\nabla \times \psi' \mathbf{k}) \cdot \nabla\left(\frac{\alpha \xi' + f'}{h'}\right) = \beta \nabla^2 \xi' - \frac{\gamma}{h'}\left[\xi' + \nabla \psi' \cdot \nabla\left(\frac{1}{h'}\right)\right] + \nabla \times \left(\frac{\boldsymbol{\tau}'}{h'}\right), \tag{6}$$

where

$$\left.\begin{aligned} \xi' &= \frac{\partial v'}{\partial x'} - \frac{\partial u'}{\partial y'} \\ \nabla &= \mathbf{i}\frac{\partial}{\partial x'} + \mathbf{j}\frac{\partial}{\partial y'} \\ \boldsymbol{\tau} &= \tau'^x \mathbf{i} + \tau'^y \mathbf{j} \end{aligned}\right\},$$

and $\mathbf{i}$, $\mathbf{j}$, $\mathbf{k}$ are the unit vectors in the right-handed x, y, z coordinate system.

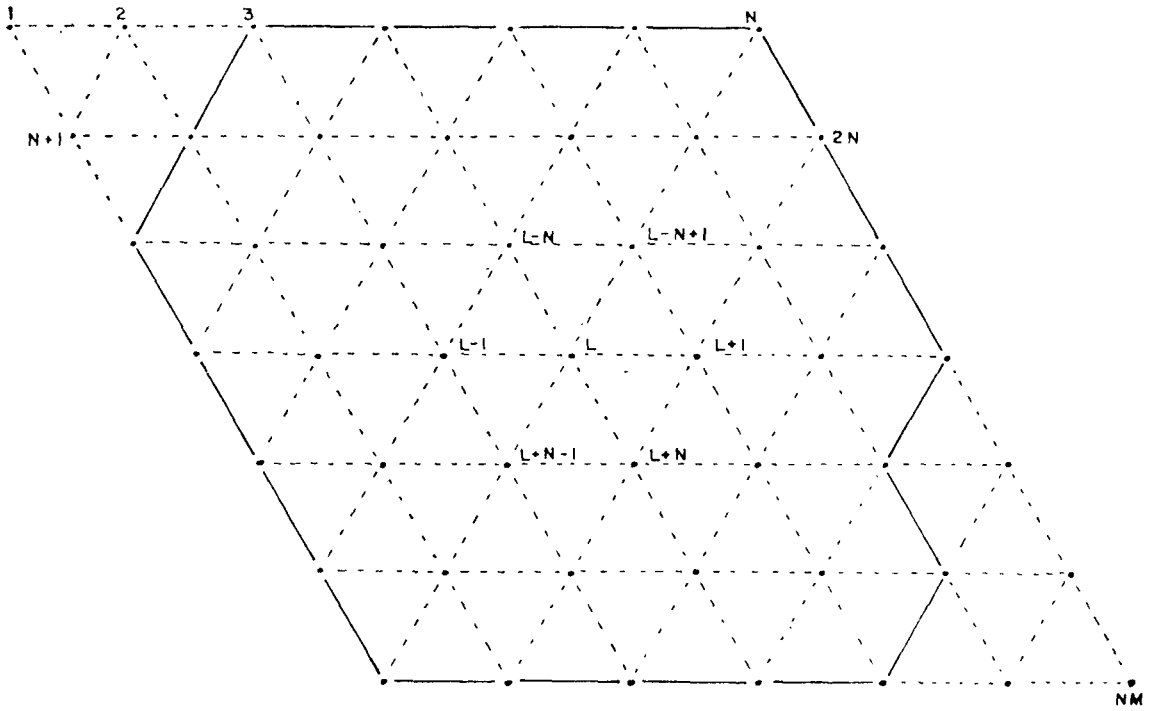

FIG. 2. Grid pattern used in finite-difference scheme and numbering system used in computational molecule.

The nondimensional constants appearing in Eq. (6) are

$$\left.\begin{aligned}\alpha&=\frac{\psi_0}{\Delta^2 DF}\\ \beta&=\frac{K}{\Delta^2 F}\\ \gamma&=\frac{R}{DF}\end{aligned}\right\}.$$

These three nondimensional parameters govern the character of the solution. For example, setting $\alpha=0$ removes the nonlinear advective terms from the model. The size of β determines how important lateral friction is in the solution, and γ scales the importance of bottom friction.

From the above we also obtain the following relationship between the vorticity and the streamfunction:

$$\nabla\left(\frac{1}{h'}\nabla\psi'\right)=\xi'. \tag{7}$$

Eqs. (6) and (7) can now be solved for the vorticity and streamfunction provided that the proper initial and boundary conditions are given. In particular the following must be specified:

(i) ψ—given within the region of interest at $t=0$
(ii) ψ—given on the boundary of the region for all time
(iii) ξ—given within the region of interest at $t=0$

Note that (ii) is equivalent to specifying the source-sink distribution around the edge of the model.

The finite-difference grid system for the model was made up of equilateral triangles with the basic computational molecule being a hexagon. Field variables were then specified as a one-dimensional array with the computational molecule again being a hexagon and a relative indexing system as shown in Fig. 2, N being the number of points in a row of the matrix of field points.

The vorticity equation was integrated forward in time using the three-level Adams-Bashforth method, and then the streamfunction was obtained with successive over relaxation techniques. All differencing was kept accurate to second order and highly conservative (Arakawa, 1966). For example, the advective terms conserved vorticity, vorticity squared, kinetic energy, kinetic energy squared, etc. The actual finite-difference equations used, the error estimates, and some results from preliminary test runs are presented by Galt (1972a).

For convenience the basic finite-difference equations that were used will be briefly outlined below. We begin by transposing the field advection term from the right-hand side to the left-hand side. The result can be written as[3]

$$\frac{\partial\xi}{\partial t}=g, \tag{8}$$

[3] From this point on the primes will be dropped and all terms will be non-dimensional unless otherwise specified.

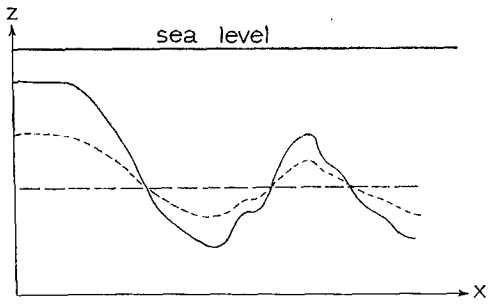

FIG. 3. Representation of scaling of bathymetry: continuous lines, actual bathymetric profile, short dashes, 50% scaled bathymetric profile, long dashes, mean depth.

where g is given by

$$g=(\nabla\times\psi\mathbf{k})\cdot\nabla\left(\frac{\alpha\xi+f}{h}\right)+\beta\nabla^2\xi - \frac{\gamma}{h}\left[\xi+\nabla\psi\cdot\nabla\left(\frac{1}{h}\right)\right]+\nabla\times\left(\frac{\tau}{h}\right). \quad (9)$$

Eq. (8) can be integrated forward in time using the difference equation

$$\xi(t+\Delta t)=\xi(t)+\left[\tfrac{3}{2}g(t)-\tfrac{1}{2}g(t-\Delta t)\right]\Delta t. \quad (10)$$

In order to use this equation we must have a finite-difference form for all of the spatial derivatives in g, the development of which will follow.

An additional feature of the numerical model was that the bathymetric variations could be scaled. One parameter was used to specify the percent of the actual bathymetric variation that was to be included for any computer run. In this way all cases from a flat bottom ocean to one with the real bathymetry (in so far as the horizontal grid could resolve it) could easily be compared. To get a better idea how this scaling works consider the bathymetry shown in Fig. 3. The actual depth is entered into the model as a mean depth and a deviation from the mean. At run time the depth in the model is taken as the mean depth plus some percentage of the deviation. Through this numerical artifact the qualitative effect of weak stratification could be simulated and the dynamic significance of bathymetric effects could easily be seen. Perhaps the major potential difficulty associated with this simplified bathymetric representation is that it does not allow for the possibility of the joint bathymetric-baroclinic interaction that Holland (1973) has shown to be of major significance in a numerical model study of the western Atlantic. The significance of this type of interaction seems to depend strongly on the overadjustment of the internal density field with the accompanying formation of a deep counter current. This could be expected where current systems are strongly nonlinear or where there is a strongly developed thermohaline circulation. In the major basins of the Arctic Ocean neither of these cases seem to develop and there has been no observation evidence of a deep counter-current system under the strongest gyre that develops in the Canadian Basin. As an additional point the preliminary results of a baroclinic model study of the Arctic Ocean done by Semtner (1973, personal communication) indicate that this joint interaction term is not of major significance. A more detailed discussion of this feature in the model is given by Galt (1972b).

We are now in a position to write down the finite-difference representation of g given in Eq. (9). Starting first with the field advection term, we have

$$\begin{aligned}(\nabla\times\psi\mathbf{k})\cdot\nabla\left(\frac{\alpha\xi+f}{h}\right) &= 3^{-3}[(\psi_{L-N+1}-\psi_{L+1})(PV_{L-N+1}+PV_{L+1})\\ &+(\psi_{L-N}-\psi_{L-N+1})(PV_{L-N}+PV_{L-N+1})\\ &+(\psi_{L-1}-\psi_{L-N})(PV_{L-1}+PV_{L-N})\\ &+(\psi_{L+N-1}-\psi_{L-1})(PV_{L+N-1}+PV_{L-1})\\ &+(\psi_{L+N}-\psi_{L+N-1})(PV_{L+N}-PV_{L+N-1})\\ &+(\psi_{L+1}-\psi_{L+N})(PV_{L+1}+PV_{L+N})], \quad (11)\end{aligned}$$

where

$$PV_I=\alpha(\xi_I)+f_I,$$

and h is the depth scaled as is indicated in the preceding paragraph.

The second term in g represents lateral friction and is written

$$\beta\nabla^2\xi=\beta\left(\tfrac{2}{3}\right)(\xi_{L+1}+\xi_{L-N+1}+\xi_{L-N}+\xi_{L-1}+\xi_{L+N-1}+\xi_{L+N}-6\xi_L). \quad (12)$$

The third term in g gives the bottom friction contribution:

$$\begin{aligned}\frac{\gamma}{h}\left[\xi+\nabla\psi\cdot\nabla\left(\frac{1}{h}\right)\right] &= \frac{\gamma}{H}\left\{\xi_L+\frac{1}{4}\left[(\psi_{L+1}-\psi_{L-1})\left(\frac{1}{h_{L+1}}-\frac{1}{h_{L-1}}\right)\right.\right.\\ &+\tfrac{1}{3}(\psi_{L-N+1}-\psi_{L+N-1}+\psi_{L-N}-\psi_{L+N})\\ &\left.\left.\times\left(\frac{1}{h_{L-N+1}}-\frac{1}{h_{L+N-1}}+\frac{1}{h_{L-N}}-\frac{1}{h_{L+N}}\right)\right]\right\}, \quad (13)\end{aligned}$$

where H is the true non-dimensional depth rather than the scaled bathymetry.

The last term in g is the rate of torque added by the

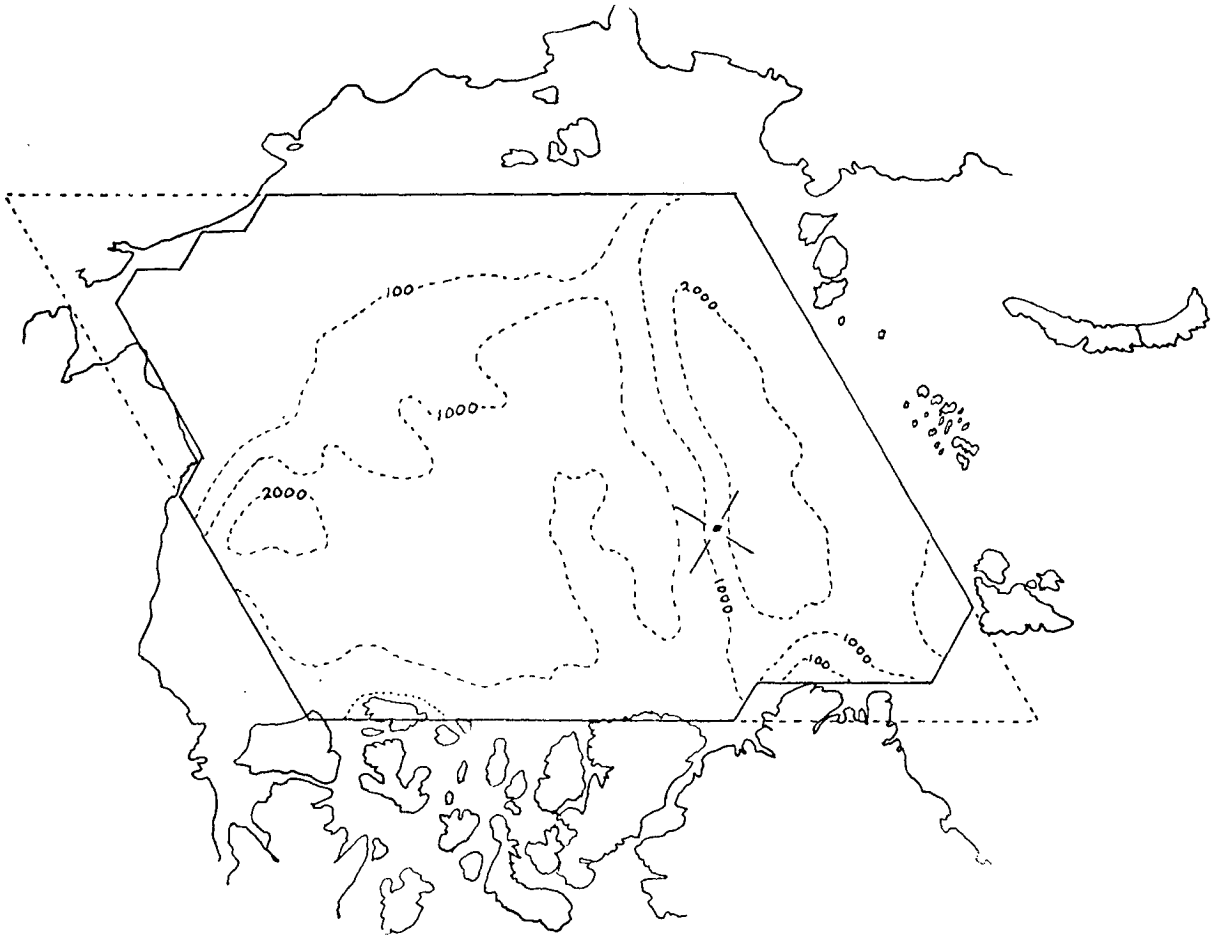

FIG. 4. Arctic configuration used in numerical model. Heavy line indicates basin shape. Dotted lines give bathymetric contours in fathoms.

wind curl:

$$\nabla\times\left(\frac{\tau}{h}\right)=\frac{1}{2}\left[\left(\frac{\mathbf{G}_2}{h}\right)_{L+1}-\left(\frac{\mathbf{G}_2}{h}\right)_{L-1}\right]-3^{-\frac{1}{2}}\left[\left(\frac{\mathbf{G}_1}{h}\right)_{L-N+1}-\left(\frac{\mathbf{G}_1}{h}\right)_{L+N}+\left(\frac{\mathbf{G}_1}{h}\right)_{L-N}-\left(\frac{\mathbf{G}_1}{h}\right)_{L+N-1}\right], \quad (14)$$

where $\mathbf{G}_1$ is the component of the wind stress in the direction from L to $L+1$ and $\mathbf{G}_2$ is the wind stress in a direction 90° to the left of $\mathbf{G}_1$.

Substituting Eqs. (11)–(14) into (9) and then into (10) a new value of the vorticity can be obtained for each grid point.

4. Description of cases studied

The numerical model contains a number of possibilities for representing various physical situations. In theory, to model the Arctic the actual oceanographic parameters are determined and inserted into the numerical model. In practice, these relevant parameters cannot be estimated with any real certainty and the appropriate course of action is to make a number of runs exploring what are thought to be the most likely regions of the parameter space. This exploration indicates the sensitivity of the model to each parameter and shows which feature of the solution is associated with particular processes.

The parameters for this model can be thought of as external, i.e., dealing with boundary conditions, or internal, i.e. dealing with the governing equations. External parameters are 1) the source-sink distribution around the edge, and 2) the surface driving stress; the internal parameters are 1) the Rossby number α, 2) the horizontal Ekman number β, 3) the bottom drag coefficient γ, and 4) the percentage of the bathymetric variation that will be included.

During the initial development of the model all of the parameters were varied over large ranges. For this presentation, however, attention will primarily be con-

FIG. 5. Contours of the curl of the wind stress obtained from average annual winds. All values are negative except where indicated positive. The maximum magnitude of the curl of the wind stress found in the Canadian Basin is 0.158×10^{-7} gm cm^{-2} sec^{-2}.

fined to Arctic cases; accordingly, the basin shape and bathymetry are held constant (Fig. 4). For this case the grid spacing was 170 km. The shape of the model was roughly that of the Arctic Ocean with a representative portion of the Siberian Shelf included. The horizontal resolution was sufficient to easily delineate the major bathymetric features.

Two different options were considered for the source-sink distribution around the edge of the model. For the first option no flow was allowed across the model boundaries. For the second option flow with no relative vorticity was specified as flowing into the model as follows (all units m^3 sec^{-1}):

1) 2×10^6 through the Chuckchi Sea
2) 2×10^6 between Franz Josef Land and Severnaya Zemlya
3) 5×10^6 in the region of the West Spitsbergen Current.

To balance this, outflow advecting whatever local vorticity was available was specified as

1) 1×10^6 through McClure Straits
2) 1×10^6 through Nares St
3) 7×10^6 through the region of the East Greenland Current.

For the surface stress driving the model there were also two options considered. For the first the wind stress field used by Campbell (1965) and representing mean annual conditions was applied to the model. For the second an ice-covered ocean was approximated by applying the above stress to an ice model developed by Campbell (*loc. cit.*) and using the water stress predicted by his results to force the ocean model. In order to indicate how these stresses are going to apply to the model we may look at Figs. 5 and 6. In these two figures the curl of the surface stress patterns for the two options is qualitatively represented. Considerable similarity is seen between these two patterns with the most conspicuous feature being the large negative rotation region centered over the Beaufort Gyre. It should be pointed out that although the patterns in these two figures have much in common the actual magnitudes associated with the under-ice stress (Fig. 5) is less by approximately a factor of 3 than the values given in Fig. 4. This seems to be due to the very large dissipation used in Campbell's model and it is likely that neither of these stress fields is quantitatively very accurate.

For each of the possible combinations of the external parameters specified above a series of cases was investi-

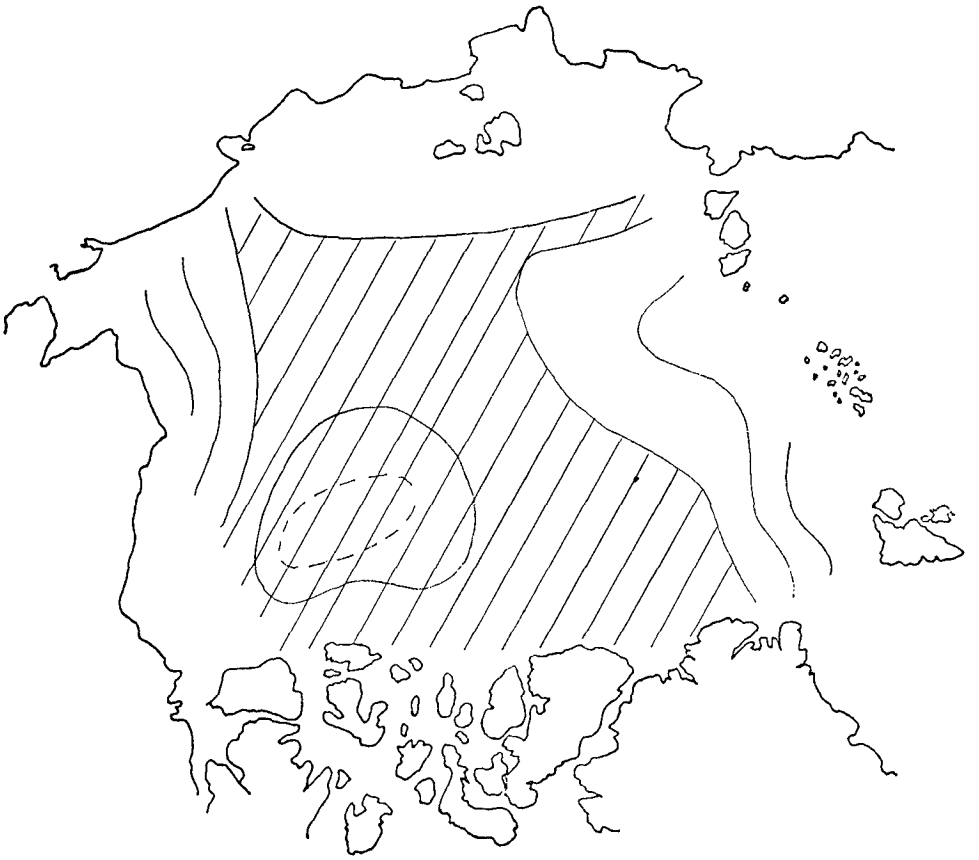

FIG. 6. Contours of the curl for the stress from the bottom of Campbell's ice model. Cross-hatched areas have negative values, all others are positive. The maximum magnitude of the curl of the ice stress found in the Canadian Basin is 0.543×10^{-8} gm cm^{-2} sec^{-2}.

gated with various combinations of the internal parameters being specified. Rather than going through and outlining all of the parameter combinations that were used, the specific combinations will be listed as each case or series is discussed in the following section.

5. Results and discussion

For all of the cases considered the ocean was initially at rest and the surface stress was turned on at time equal zero. As the model spun up the total kinetic energy of the flow was monitored both to check the stability of the numerical scheme and to get an indication of whether a steady state was being approached. The energy vs time curves looked similar for all cases and showed a rapid buildup of kinetic energy at first and finally an asymptotic approach to a steady value after large time. This in itself is nothing new and almost all numerical ocean models with modest Rossby numbers exhibit qualitatively the same sort of behavior. There were, however, two things about these curves that did make them different. First of all the curves were quite smooth and didn't show any overshoot and oscillations as are typical of models without excessive damping and shown, for example, in Bryan (1963). The second point was that a relatively long time was required for the model to come to steady state. After one year the kinetic energy was only to 80% of its final value, with the corresponding value for two years being 97% (Fig. 7).

To explain this apparent difference it is necessary to consider the mechanics of the spin-up process. The

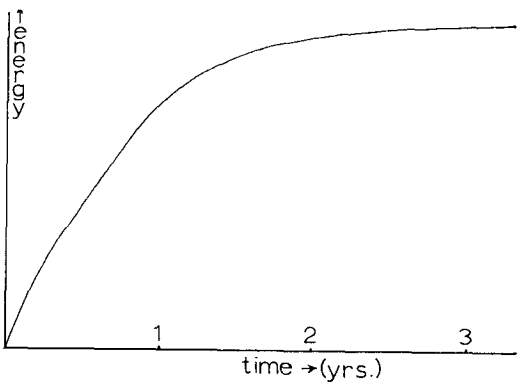

FIG. 7. Total kinetic energy within the model as a function of time for a wind-driven nonlinear case that includes inflow-outflow and both bottom and lateral friction.

initial adjustment of vorticity is carried out via transient Rossby waves: either those whose dynamics is controlled by the change of the Coriolis parameter with latitude, or those controlled by topographic variations (Veronis, 1966). In a polar ocean the variation of the Coriolis parameter is very much less than at low latitude (typically an order of magnitude with the variation actually being zero at the pole). Thus, the usual Rossby waves will have much slower propagation speeds than in low latitudes and transients could be expected to develop more smoothly. This is, in fact, verified by a close look at the model output and will be discussed later. It also appears that the effective bathymetry will not cause sufficient development of topographic Rossby waves with speeds comparable to those that dominate the spin-up in lower latitude oceans.

In order to check these ideas the model was reconfigured for a four-sided, flat-bottomed, mid-latitude ocean and forced with a cosine-dependent, zonal surface stress as was used by Bryan (1963). In this case the spin-up took on the order of 20–40 days. The kinetic energy showed an overshoot and oscillated around the ultimate mean value. The development of a western boundary current was similar to that shown by Bryan. It therefore seems that the smooth, slow adjustment of the Arctic model is in fact related to its high latitude and effective bathymetric variations.

A better indication of the actual spin-up of the model can be obtained by looking at the time development of the streamline patterns. Starting with a particularly simple case the model was configured for a flat bottom with no inflow-outflow around the edges. There were no nonlinearities included ($\alpha=0$). Parameter β was taken so as to have a horizontal eddy coefficient of 10^7 cm^2 sec^{-1}. The model was driven by the annual average wind stress pattern. The dynamics in the model corresponds to a time-dependent version of Munk's ocean circulation model (1950).

The major source of wind torque is in the Beaufort Sea and it is here that initial Rossby wave first starts to form. After its formation it propagates roughly westward or over toward the western boundary to establish a Gulf-Stream-like current along the Siberian Coast. The streamline pattern after 300 days is shown in Fig. 8. This clearly shows the development of a western boundary current similar to other models with lateral friction and no nonlinearities. The progress of the center of the gyre is shown by the dotted line in

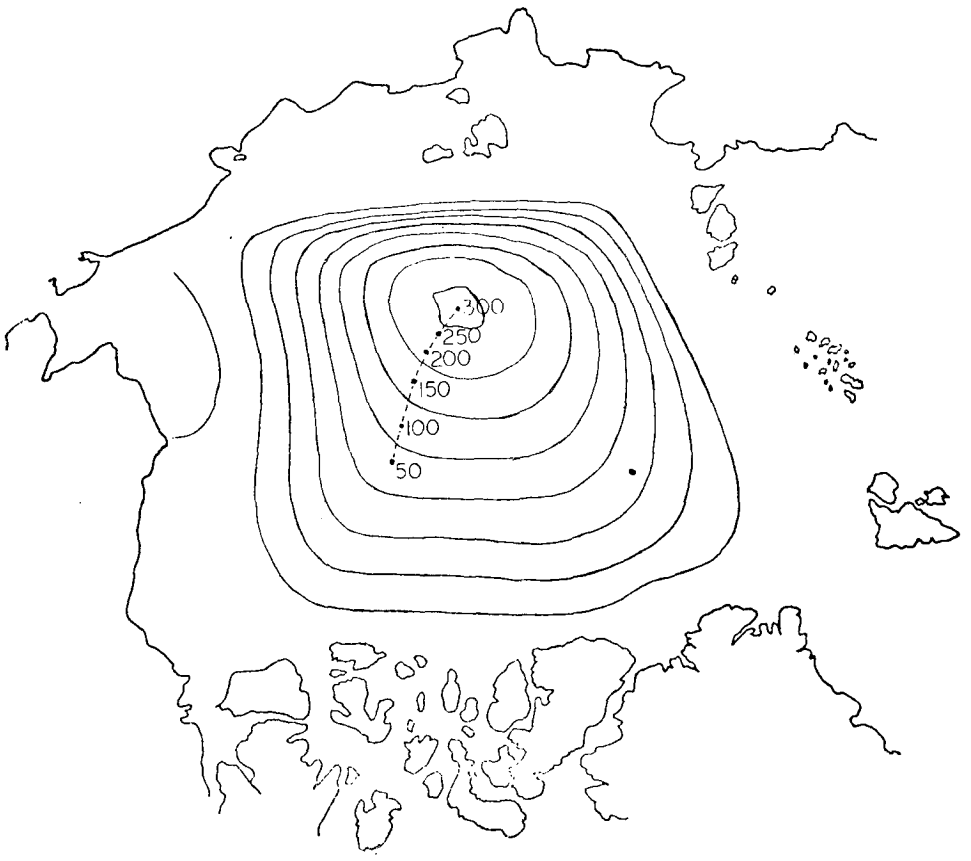

FIG. 8. Streamline pattern for wind-driven flow at 300 days into the spin-up. For this case the model was linear, had a flat bottom, with no bottom friction, or inflow-outflow around the edges. Dotted line indicates the trajectory of the center of the gyre with the time given in days. Between solid lines the transport is 10^7 m^3 sec^{-1}.

Fig. 8 with the time into the model given in days. From these it is possible to calculate the speed of propagation of the gyre, i.e., $\sim$6 km day^{-1} between 50 and 150 days. If one assumes that the gyre represents a simple Rossby wave then the phase velocity to the west will be given by

$$\frac{\partial f}{\partial y}\frac{1}{|\mathbf{k}|^2},$$

where y is the local north-south coordinate and $|\mathbf{k}|$ the magnitude of the wavenumber. Putting in the appropriate numbers suggests a wavelength of a little over 1000 km and considering the irregularities of the basin shape and the numerical methods used this is not a bad approximation for the size of the gyre during its initial period of development. For this simple case, then, the major transient appears to be a Rossby wave that develops under the torque source of the wind and propagates to the western boundary region adjacent to the Siberian coast.

The next series of cases investigated with the model looked at the effects of bathymetric variations. In all cases the actual bathymetry of the Arctic was specified as 3000 m plus a residual. This residual was then multiplied by a coefficient that varied between 0.0 and 1.0. Thus, a coefficient of zero was equivalent to a flat bottom ocean, a value of 0.5 was equivalent to including 50% of the bathymetric variation, etc. (Fig. 4).

The models of this series included lateral friction, bottom friction, nonlinearities, and sources and sinks around the edges. Cases with 0 to 100% bathymetry were run. We may start off by looking at the kinetic energy of the flow after 300 days (Fig. 9). Here the effect of bathymetry in reducing the flow is clearly seen. It shows that very small bathymetric variations quickly reduce the magnitude of the flow, after which continuing to increase the bottom topography continues to slowly decrease the flow. This is consistent with studies by Schulman and Niiler (1970).

A better indication of the dynamics associated with these cases can be obtained by looking at the actual time development of the streamline patterns. For the flat bottom case a western boundary current develops along the Siberian Coast similar to that shown in Fig. 8. With any bathymetry at all the possibility of topographic Rossby waves is introduced (Veronis, 1966) and these can be expected to play some role in the development of the flow pattern.

The Lomonosov Ridge (Fig. 1) cuts the Arctic into two basins and runs essentially directly across the pole. In this region the variation of the Coriolis parameter is zero and any topographic Rossby waves that occur will dominate the transients in the solution. The major vorticity source due to the wind is on the Canadian side of the ridge and waves that develop here will propagate counterclockwise (or to the left looking up hill). In this way the initial waves move toward the Siberian Shelf relatively rapidly due to the steepness of the ridge. In essence the ridge acts as a dynamic block and almost none of the vorticity delivered to the ocean in the Canadian Basin propagates across the Lomonosov Ridge and ends up on the Eurasian side. This explains the substantial drop in kinetic energy between the flat bottom case and the 5% bathymetry case, i.e., much less water actually ends up moving.

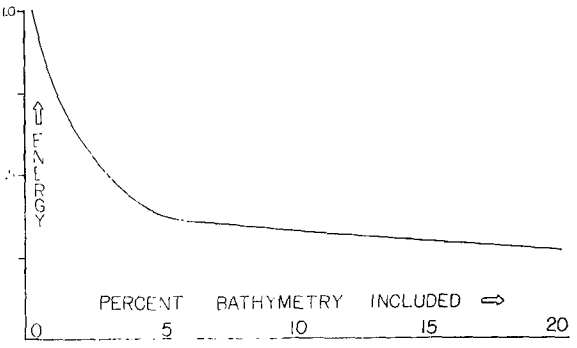

FIG. 9. Qualitative representation for the total kinetic energy of the flow at 300 days into the model (normalized with respect to the flat bottom case) versus the percent of bathymetric variation included. This configuration included nonlinear terms, lateral and bottom friction, as well as inflow-outflow on the boundaries.

As the gyre forming in the Canadian basin grows it expands along the Lomonosov Ridge and encounters the second major feature of the bathymetry, the continental slope adjacent to the Siberian Shelf. At this point, if bathymetry were dominating the transients, the gyre would move, again to the left looking uphill, or over toward the coast of Alaska. The speed of propagation of waves along the continental slope would be slower than along the Lomonosov Ridge because of smaller slopes.

For 5% of the bathymetry the major topographic features of the Arctic are clearly seen to influence the initial development of the solution (Fig. 10). The ridge confines the flow primarily to the Canadian side of the Lomonosov Ridge. The gyre that is initially formed in the Beaufort Sea moves relatively rapidly (compared to the flat bottom case) toward the New Siberian Islands and expands in size. Upon reaching the continental slope the gyre tends to migrate toward the North Coast of Alaska, but with only 5% of the bathymetry the topographic effects don't totally dominate and two regions of weakly concentrated currents develop as the solution approaches steady state—one along the Siberian Coast (western boundary current region) responding to the variation of the Coriolis parameter and a second along the north coast of Alaska responding to the topographic variations.

For 10% of the bathymetry the results are qualitatively similar to the 5% case initially, but a number of differences are seen in the details. First of all the transients propagate slightly faster as would be ex-

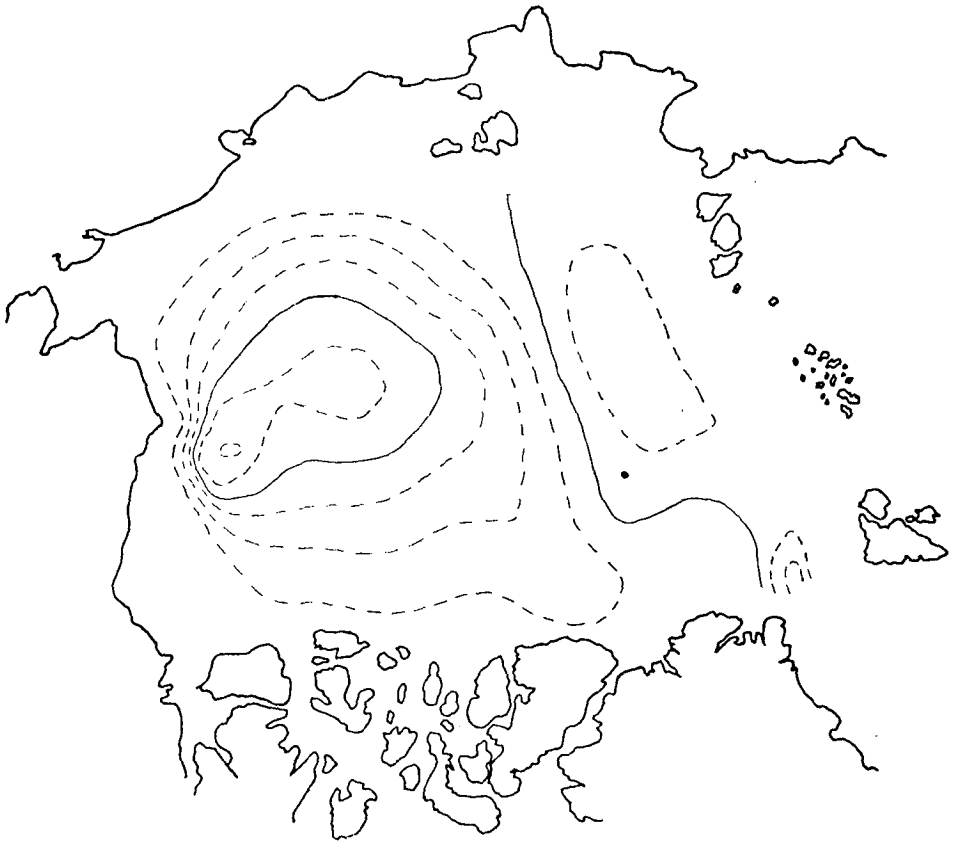

FIG. 10. Streamline pattern for ice driven flow at 300 days into spin-up. Nonlinear terms, bottom and lateral friction, inflow-outflow on the boundaries, and 5% of the bathymetric variation are included. Between solid lines the transport is 10^7 m^3 sec^{-1}.

pected. In addition, the topographic effects are now clearly seen to dominate and there is no tendency for a concentrated flow to develop along the Siberian Coast. The boundary current is now controlled by depth variations, rather than variations in the Coriolis parameter. It occurs along the north coast of Alaska, i.e., the Barrow Current. Another noticeable characteristic of the flow is the response to secondary topographic features. Meanders appear just downstream from the Chuckchi Rise and the Alpha Rise (Fig. 11).

The transients generated by the spin-up exhibit some interesting features as they are advected by the mean flow. The transients propagate counterclockwise against the clockwise gyre that is developed. Initially their net motion is upstream everywhere, but as the gyre speeds up the waves first become stationary in some regions and then show actual downstream motion until a steep enough slope region is encountered so that they can again be phase locked or at least quasi-stationary. These transient motions are clearly seen in a time-lapse development of the solution. The waves tend to end up where the mean circulation turns off of the continental slope region and moves along the steeper face of the Lomonosov Ridge (Fig. 11). After the solution has come approximately to steady state (one year), these waves are seen to shift back and forth slightly along the face of the Siberian slope and Lomonosov Ridge. Ultimately the bottom friction damps them out even in these deeper portions of the basin and the streamline pattern becomes quite stationary (on the order of a three-year time scale for the bottom friction used in the model).

Increasing the bathymetric variation to 20% reduces the energy of the flow somewhat, but not very drastically. In this case, however, secondary bathymetric features cause significant effects on the flow (Fig. 12). For example, a large closed gyre forms between the Alpha Rise and the Lomonosov Ridge. Going to full bathymetric variations gives even greater reductions in the flow with streamlines pretty much following the bathymetry.

Summarizing the results from the investigation of the topographic features, it appears that the most realistic flow patterns occur when about 10% of the bathymetric variations are included in the model. In this case topographic Rossby waves play a fundamental roll in the development of the current patterns. The physical interpretation of this clearly numerical artifact is as follows. If the ocean is highly stratified the baroclinic and barotropic horizontal pressure gra-

FIG. 11. Streamline pattern for the wind-driven case after 600 days. Non-linear terms, bottom and lateral friction, inflow-outflow on the boundaries, and 10% of the bathymetric variation are included. Between solid lines the transport is 10^7 m^3 sec^{-1}.

dients tend to cancel each other out at depth and a "level of no motion" occurs. If this level is above the major topographic features the bathymetry has a minimal effect on the large-scale circulation. In such cases the dynamics will be controlled by variations in the Coriolis parameter and a flat-bottom homogeneous model will give reasonable results. On the other extreme a homogeneous ocean will have flow that is barotropic and all of the topographic features will influence the flow. In this case a homogeneous ocean model with realistic bathymetry could be expected to give reasonable results.

The Arctic is somewhere between these two extreme cases, having relatively weak stratification and substantial bathymetric variations. Here then a successful model might be expected to result from a homogeneous formulation and reduced bathymetric variations. Some qualifications will obviously be needed on the success. For example, one would not expect the phase velocities and ultimate wavelengths of the transient topographic Rossby waves to be accurately represented. In addition, certain baroclinic-bathymetric interactions (Holland, 1972) cannot be represented in the model as was discussed in Section 3. Subject to these limitations the model may be useful in showing some of the dynamics that tend to control the Arctic circulation. Before pursuing this in greater detail the effects of source and sinks around the boundary, bottom friction, and nonlinearities will be discussed.

On the Canadian side of the Arctic the inflow-outflow across the boundaries is relatively weak (2×10^6 m^3 sec^{-1} in through the Chuckchi Sea and out through the Canadian Archipelago) and the wind-driven circulation is relatively strong. For all the cases tested the source-sink driven flow didn't cause any significant modifications to the dominant wind-driven circulation.

In the Eurasian Basin side of the Arctic the inflow-outflow across the boundaries is stronger and the wind-driven flow weaker than on the Canadian side. Here the inflow-outflow can be seen to modify the wind-driven circulation. The relatively weak anticyclonic winds on the Eurasian side of the Arctic form a small clockwise gyre that migrates to the left along the Eurasian face of the Lomonosov Ridge and ends up NNE of Greenland (Fig. 11). The source-sink driven flow moves counterclockwise around Spitsbergen and tends to flatten the wind-induced gyre and compress it towards the Lomonosov Ridge. It should be pointed

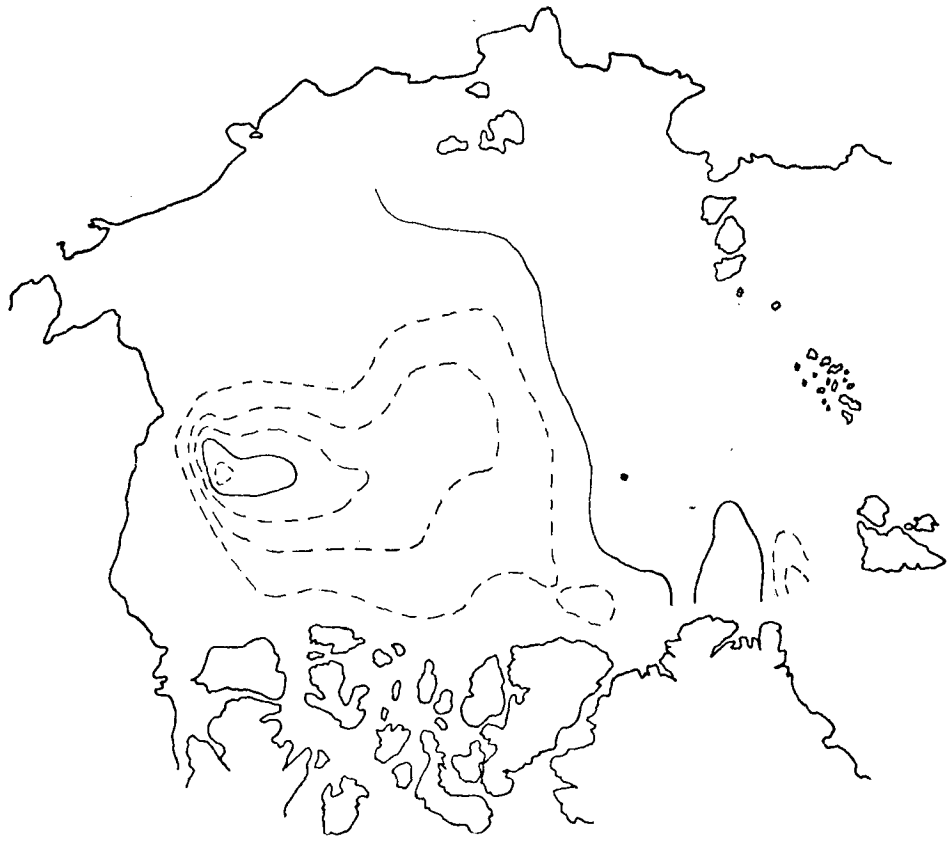

FIG. 12. Streamline pattern for a case identical to the one shown in Fig. 10 except that 20% of the bathymetric variation is included.

out that the inflow-outflow between Spitsbergen and Greenland is strongly baroclinic and any further extension of these model results are not likely to be significant.

Bottom friction is included in the model as a simple linear drag term. This would result in an exponential decay of the flow in the absence of all other forcing. The frictional coefficient then can be easily parameterized in terms of the time required for an *e*-folding decay of the current. The decay times were directly proportional to the actual depth so the times given are for 50 m deep water on the Siberian Shelf. Decay times for 2.5, 10 and 20 days were tried for representative ranges of the other parameters. For the 2.5-day decay time the circulation was greatly reduced over the entire basin. A 10-day decay time greatly reduced the flow in the region of the shelf and smoothed the streamlines over the continental slope region. For a 20-day decay time the flow was slowed down considerably over the shelf; somewhat damped topographic Rossby waves could be seen in the solution over the continental slope (transients significantly damped in three years), and the flow in the deeper basins was essentially unaffected (Fig. 11). For this value of decay the corresponding *e*-folding time for the deep part of the Canadian Basin would be over 1500 days, or long compared to the spin-up time for the circulation. This of course means that for most of the cases shown the model was not run to a completely stationary solution. This was done in an effort to save computer time and in no case were the transients at one year into the model a significant part of the circulation. For example, the results shown in Fig. 11 for 600 days are in no way significantly different from the results at 1200 days. (The kinetic energy vs time for this case is shown in Fig. 7.)

The nonlinear advective terms had very little effect over most of the region in the model. When they were included the total transport in the Beaufort Gyre was slightly reduced. The thickness of the boundary layer along the Alaskan coast was increased and the region of maximum flow moved approximately one grid length downstream, or toward the west.

At this point it is interesting to look at Fig. 13 which gives the dynamic height contours and inferred circulation in the Beaufort Gyre as calculated by Coachman (1969). This circulation pattern was obtained from a number of hydrographic stations scattered over the area and taken over a period of many years. A comparison of this figure with the model results shown in Fig. 11 should yield some useful dynamic insights.

A number of similarities can be noted: 1) the roughly triangular shape of the most intense part of the gyre,

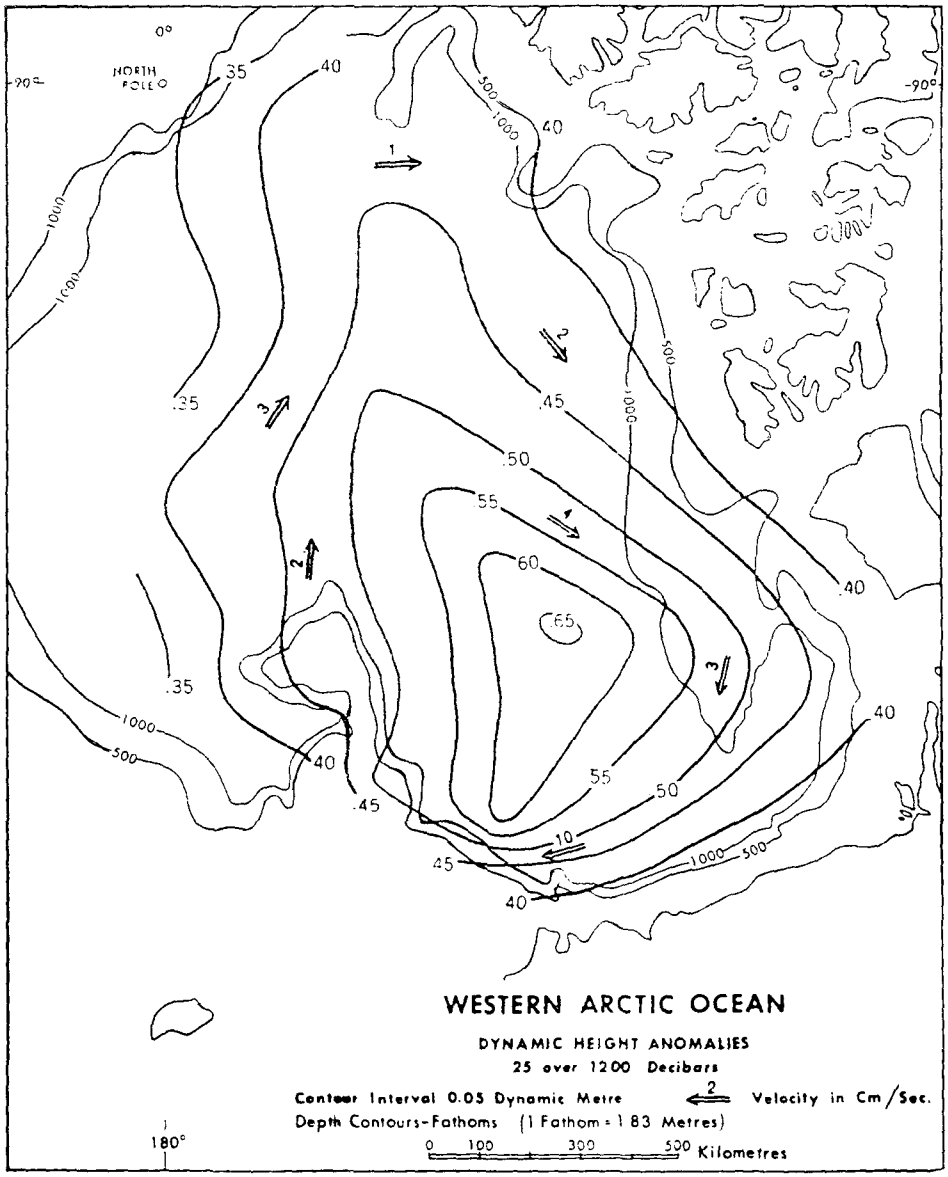

FIG. 13. Dynamic topography and inferred circulation for the Canadian Arctic (after Coachman, 1969).

2) the strongest currents found just north of Pt. Barrow, 3) meander patterns associated with the Chuckchi Rise and the Alpha Rise, and 4) wave patterns seen where the flow crosses the continental slope and moves along the Lomonosov Ridge. In these respects the model has successfully simulated some of the major flow characteristics in the Canadian Arctic Basin.

A final series of runs was made using a surface stress field that was obtained from the underside of a model of ice circulation developed by Campbell (1972, personal communication). The ice model was in turn driven by the same wind stress field that was used for the previously discussed cases. The object here was to see how sensitive the ocean model was to the details of the stress field, and to attempt to represent some of the filtering effects that the ice cover might have. The curl of the stress field is shown in Fig. 6.

Fig. 14 shows the streamline pattern after 600 days for the case that includes inflow-outflow, bottom friction, lateral friction and nonlinearities. This corresponds to the results shown in Fig. 11 in every respect except for the driving stress pattern. In the Canadian Basin the flow is qualitatively very similar with the actual magnitude of the flow in the ice stress case being about half what it was for the wind stress case. If the appropriate transports in the current off the coast of Alaska are converted to representative velocities, values of between 5 and 12 cm sec^{-1} are obtained. These are in

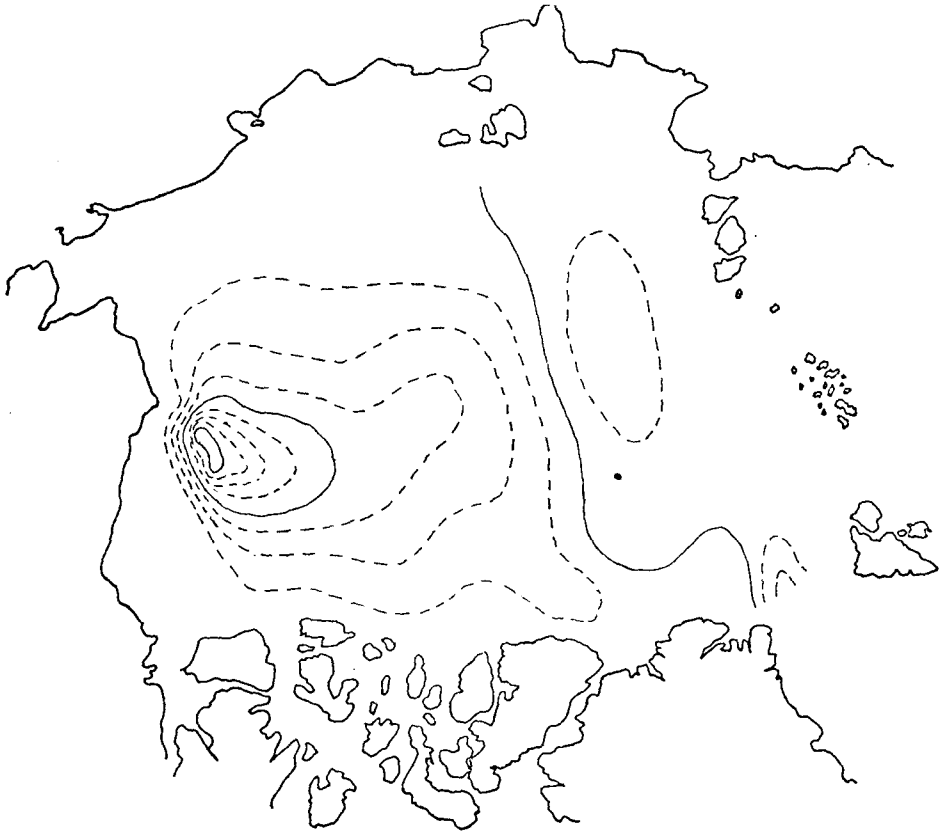

FIG. 14. Streamline pattern for the ice stress driven case after 600 days. All other parameters are identical to those shown in Fig. 11.

acceptable agreement with those shown by Coachman (Fig. 13).

On the Eurasian side of the Lomonosov Ridge the net effect of the surface torque is counterclockwise for the ice stress (compare Figs. 5 and 6) and a correspondingly weak counterclockwise gyre is formed instead of the weak clockwise one that was formed using just wind stress values. It is unknown which of these is more correct. Surface drift data would tend to favor the ice stress driven flow (Fig. 14) whereas the total integrated transport may be more like what is shown in Fig. 11.

In general it seems that the actual pattern of the major wind-driven flow (on the Canadian side of the Lomonosov Ridge) is insensitive to the details of the applied stress pattern, although the magnitude of the circulation does show some of the response to changing the stress. This is, of course, consistent with other studies of ocean circulation that have been conducted on mid-latitude oceans. (For example, the position of the Gulf Stream doesn't depend very strongly on the details of the tradewinds). The major difference for the Arctic case is that the current is not set up by Rossby waves that lead to a western boundary current, but rather by bathymetric effects with the strong current forming to the left looking upslope from the major torque source in the Canadian Basin to the dominant topographic feature (the Siberian Shelf). This then is a major ocean current system where topographic Rossby waves play the fundamental roll in the establishment and maintenance of the current patterns.

6. Conclusions

A barotropic model of the Arctic Ocean with reduced bathymetric contrast can successfully represent some of the major features of the circulations. This suggests that while baroclinic effects are of some importance in the Arctic the large-scale circulation is dominated by the bathymetry. The study also seems to indicate that the joint bathymetric-baroclinic interaction terms are not of major significance. This is different from the western boundary current system seen in the Atlantic (and presumably the Pacific). It is suggested that this difference may be due to the lack of strong deep thermohaline circulations or significant nonlinear effects in the Arctic Basins. The major bathymetric features of the Arctic Ocean that are seen to influence the flow are 1) the Lomonosov Ridge that runs nearly across the pole and divides the Arctic into the Canadian and Eurasian sides, and 2) the Siberian shelf/continental slope that

gives a relatively gradual (by dynamically significant) slope to the Siberian side of the Canadian Basin. In addition to these major features there are two secondary bathymetric features that modify the circulation—the Chuckchi Rise and the Alpha Rise.

In the Arctic the variation of the Coriolis parameter is small and the fact that bathymetry dominates the general circulation is really equivalent to the statement that topographic Rossby waves take over the role that classical Rossby waves play in the development and maintenance of the general circulation in mid-latitude oceans. This has considerable implications on the details of how the bathymetric variations actually control the flow.

The major source for vorticity in the Arctic is the negative wind curl region in the Beaufort Sea. The Lomonosov Ridge acts as a dynamic block and the transients generated in this source region are generally confined to the Canadian side. In the initial spin-up the transient topographic Rossby waves are seen to propagate counterclockwise along the face of the Lomonosov Ridge. As the gyre in the Beaufort Sea enlarges to cover the entire Canadian basin, the decrease in depth toward the Siberian Shelf and continental slope has dynamically the same effect as an increase in the Coriolis parameter would have in a mid-latitude flat-bottom ocean. The result is an intensification of the current to the left looking up hill and a boundary current is formed (analogous to a western boundary current). In this case the boundary current occurs along the North Coast of Alaska. Frictional and nonlinear dissipation in the boundary current region develop the vorticity sink that ultimately establishes the steady-state circulation. The nonlinear effects in the currents seem to be minimal and do little more than slightly increase the thickness of the boundary layer and shift its region of maximum intensity down stream to a point roughly north of Pt. Barrow, Alaska.

The secondary bathymetric features are responsible for initiating quasi-stationary meanders in the major gyre that is formed. These appear as wavelike patterns just downstream from the Alpha Rise and the Chuckchi Rise. Quasi-stationary wave patterns also develop where topographic Rossby waves turn along the continental slope as they come off the Lomonosov Ridge. In this area the phase velocity of waves undergoes a change and it is possible for them to become phase locked by the advection of the mean flow.

Bottom friction effectively reduces the flow over the Siberian Shelf but has no noticeable influence on the flow in deeper portions of the Basins. Increasing the significance of bottom friction is seen to suppress the quasi-steady waves that form along the continental slope.

The flow driven by the source-sink distribution simulating the major channels into and out of the Arctic Ocean have a negligible contribution on the Canadian side of the Lomonosov Ridge where the wind driven circulation dominates by at least an order of magnitude. On the Eurasian side of the Lomonosov Ridge the inflow-outflow is much greater and the wind-driven component of the flow much smaller than the corresponding components on the Canadian side. Consequently, here the source-sink driven flow is a significant contributor to the total circulation. Because of the baroclinic nature of the actual inflow-outflow of the Eurasian basin it is not clear how accurate the details of the model results are in this region.

Simulating the effect of an ice cover with a modified stress field indicates that the circulation is quantitatively but not qualitatively sensitive to the details of the applied stresses. Changing the net sign of the local wind curl does lead to a reversal of the circulation in the Eurasian basin.

The interesting question of the response of the ocean to stresses with length scales short enough to generate a strongly baroclinic flow remains unanswered. This may represent a problem of unique relevance to ice-covered oceans where mechanical failures of the ice pack, or polyna formation could supply the necessary stress distributions.

Acknowledgments. This research was funded by the Arctic Section of the Office of Naval Research.

REFERENCES

Aagaard, Knut, 1966: The East Greenland Current north of the Denmark Strait. Ph.D. thesis, University of Washington, 83 pp.

Arakawa, Akio, 1966: Computational design for long-term numerical integration of the equations of fluid motion: Two-dimensional incompressible flow. Part 1. *J. Comput. Phys.*, **1**, 119–143.

Bryan, Kirk, 1963: A numerical investigation of a nonlinear model of a wind-driven ocean. *J. Atmos. Sci.*, **20**, 594–606.

Bushuyev, A. V., N. A. Volkov, Z. M. Gudknvick and V. S. Loshchilov, 1967: Results of expedition investigations of the drift and dynamics of the ice cover of the Arctic Basin during Spring 1961. (Article summarized and reviewed by H. Solomon and S. Olenicoff and reprinted in AIDJEX Bull. No. 3.)

Campbell, William J., 1965: The wind-driven circulation of ice and water in a polar ocean. *J. Geophys. Res.*, **70**, 3279–3301.

Coachman, L. K., 1969: Physical oceanography in the Arctic Ocean: 1968. *Arctic*, **22**, 214–224.

——, and C. A. Barnes, 1961: The contribution of the Bering Sea water to the Arctic Ocean. *Arctic*, **14**, 147–161.

——, and ——, 1963: The movement of Atlantic water in the Arctic Ocean. *Arctic*, **16**, 9–16.

Galt, J. A., 1967: Current measurements in the Canadian Basin of the Arctic Ocean. Summer 1965. Tech. Rept. No. 184, Dept. of Oceanography, University of Washington.

——, 1972a: The development of a homogeneous numerical ocean model for the Arctic Ocean. Naval Postgraduate School Report (AD 744925).

——, 1972b: Numerical simulation of Arctic Ocean dynamics. *Proc. 1972 Summer Computer Simulation Conf.*, Vol. II, San Diego, Calif., 948–952.

Holland, W. R., 1967: On the wind-driven circulation in an ocean with bottom topography. *Tellus*, **19**, 582–600.

——, 1972: Energetics of baroclinic oceans. *Proc. Numerical Models Symp.* Durham, N. H., Natl. Acad. Sci. (in press).

——, 1973: Baroclinic and topographic influences on the transport in western boundary currents. *Geophys. Fluid Dyn.* (in press).

Holton, James R., 1965: The influence of viscous boundary layers on transient motions in a stratified rotating fluid: Part I. *J. Atmos. Sci.*, **22**, 402–411.

Maykut, Gary A., and Norbert Untersteiner, 1971: Some results from a time-dependent thermodynamic model of sea ice. *J. Geophys. Res.*, **76**, 1550–1575.

Munk, W. H., 1950. On the wind-driven ocean circulation. *J. Meteor.*, **7**, 79–93.

Nikitin, M. M., and N. I. Dem'yanov, 1965: O glubinnikh techeneyakh Arkticheskogo Passeina. *Okeanologiya*, **5**, 261–263.

Rothrock, D. A., 1972: Circulation of an incompressible ice cover. Paper presented Symp. Air-Sea Interaction in Polar Regions, Annual Fall meeting Amer. Geophys. Union (abstract, *Trans. AGU*, **53**, 1010).

Sadourny, Robert, Akio Arakawa and Yale Mintz, 1967: Integration of non-divergent barotropic vorticity equation with an icosahedral-hexagonal grid for the sphere. Tech Rept. No. 2, Dept. of Meteorology, UCLA.

Schulman, Elliott E., and Pearn R. Niiler, 1970: Topographic effects on the wind-driven ocean circulation. *Geophys. Fluid Dyn.*, **1**, 439–462.

Semtner, Albert J., 1972: A numerical investigation of Arctic Ocean circulation. Paper presented Symp. Air-Sea Interaction in Polar Regions, Annual fall meeting Amer. Geophys. Union (abstract, *Trans. AGU*, **53**, 1015).

Somov, M. M., Ed., 1954–55: *Observational Data of the Scientific-Research Drifting Station of 1950–1951*, Vol. 1. Morskoi Transport, Leningrad.

Veronis, George, 1966: Rossby waves with bottom topography. *J. Marine Res.*, **24**, 388–394.

——, and Henery Stommel, 1956: The action of variable wind stresses on a stratified ocean. *J. Marine Res.*, **15**, 43–75.

Williamson, David L., 1968: Integration of the barotropic vorticity equation on a spherical geodesic grid. *Tellus*, **20**, 624–653.

Witting, James, 1972: Arctic ice circulation model. Paper presented Symp. Air-Sea Interaction in Polar Regions, Annual fall meeting Amer. Geophys. Union (abstract, *Trans. AGU*, **53**, 1016).